NASA Technical Memorandum 4522

Energy-Loss Cross Sections for Inclusive Charge-Exchange Reactions at Intermediate Energies

Francis A. Cucinotta,
Lawrence W. Townsend,
and Rajendra R. Dubey

OCTOBER 1993

NASA Technical Memorandum 4522

Energy-Loss Cross Sections for Inclusive Charge-Exchange Reactions at Intermediate Energies

Francis A. Cucinotta,
and Lawrence W. Townsend
Langley Research Center
Hampton, Virginia

Rajendra R. Dubey
Old Dominion University
Norfolk, Virginia

Abstract

Charge-exchange reactions for scattering to the continuum are considered in a high-energy multiple-scattering model. Calculations for (p,n) and $(^3He,^3H)$ reactions are made and compared with experimental results for ^{12}C, ^{16}O, and ^{27}Al targets. Coherent effects are shown to lead to an important role for inelastic multiple-scattering terms when light projectiles are considered.

Introduction

In high-energy proton collisions, several mechanisms lead to secondary neutron production. Low-energy neutrons are produced in evaporation processes. At somewhat higher energies, secondary neutrons from intranuclear cascades are produced. Neutrons are also produced near the incident proton energy from charge-exchange reactions that can occur with or without concomitant pion production. These sources of high-energy neutrons may be important for risk assessments of space radiation to astronauts. The relative biological effectiveness (RBE) of high-energy neutrons has not been studied in great detail; however, one study with neutrons near 400 MeV (ref. 1) indicates a biological effectiveness similar to that of 14-MeV neutrons with values of RBE between 10 and 30. Because galactic cosmic ray fluxes are dominated by high-energy protons, an accurate prediction of secondary neutron sources is then required for proper risk assessment.

In this paper we present a model for neutron production from charge-exchange processes at intermediate energies in proton-nucleus reactions. Protons and neutrons may be considered as a single particle with an intrinsic degree of freedom called "isospin," which is analogous to the more familiar spin degree of freedom. The charge exchange then corresponds to an isospin transition or isospin flip between target and projectile nucleons. Neutron production with concurrent pion production (e.g., through isobar formation) will be considered elsewhere. From general principles, the free nucleon-nucleon (NN) amplitude for charge exchange (f_{ex}) is written in terms of the proton-proton (pp) and neutron-proton (np) amplitudes as

$$f_{ex} = f_{pp} - f_{np} \tag{1}$$

At high energies (>1 GeV), f_{pp} and f_{np} become approximately equal (ref. 2) and one should expect only a small contribution from elastic nucleon events in the nucleus unless nuclear medium modifications alter these amplitudes drastically from their free values. We have described a model of inclusive (IN) nuclear reactions for high-energy reactions that has been successful in describing momentum distributions for proton and alpha-particle reactions (refs. 3–5). We apply this model to the charge-exchange reaction

$$p + T \rightarrow n + X \tag{2}$$

at intermediate energies where f_{ex} is not negligible. The same model applies to a charge exchange for neutron projectiles and also to a charge exchange for the mass number $A = 3$ nuclei (e.g., $^3\mathrm{He} + T \rightarrow {}^3\mathrm{H} + X$). In the remainder of this paper we present our formalism for charge-exchange reactions in inclusive scattering. Physical inputs for our calculations are then described, including a description of fits to experimental data for nucleon-nucleon scattering that is used to make absolute predictions for nucleon-nucleus reactions. Illustrative calculations of the model are then discussed and compared with experiments and, finally, conclusions are made.

Inclusive Scattering Model

The differential cross section in energy loss and scattering angle for inclusive reactions may be written (refs. 3–5) as

$$\frac{d^2\sigma}{d\Omega\ dE_{P'}}\Big)_{\rm IN} = \frac{k^2}{(2\pi)^2}\int d^2b\ d^2b'\ e^{i\mathbf{q}\cdot(\mathbf{b}-\mathbf{b}')}e^{i\left(\chi(\mathbf{b})-\chi^\dagger(\mathbf{b}')\right)}\sum_{m=1}^{A_T} W_m\left(\mathbf{b},\mathbf{b}',\omega\right) \tag{3}$$

After angular integration the energy-loss cross section is

$$\frac{d\sigma}{dE_{P'}}\Big)_{\rm IN} = \int d^2b\ e^{-2Im\,\chi(\mathbf{b})}\sum_{m=1}^{A_T} W_m\left(\mathbf{b},\mathbf{b},\omega\right) \tag{4}$$

where $\mathbf{b}$ and $\mathbf{b}'$ are impact parameter vectors, $\mathbf{q}$ is the momentum transfer vector, k is the relative wave number, χ is the eikonal mean-field potential, and the energy loss is $\omega = E_P - E_{P'}$, where E_P and $E_{P'}$ are the initial and final projectile energies. The collision terms in equations (3) and (4) are defined as

$$W_m\left(\mathbf{b},\mathbf{b}',\omega\right) = \frac{1}{(m!)^2}\int\prod_{j=1}^{m}\left[\frac{d\mathbf{k}_j}{(2\pi)^3}\right]\delta\left(E_f - E_i\right) < 0_P 0_T\left|\left(\widehat{\chi}\left(\mathbf{b}\right)\right)^m\right| 0_P\mathbf{k}_j >$$

$$\times < \mathbf{k}_j 0_P\left|\left(\widehat{\chi}^\dagger\left(\mathbf{b}'\right)\right)^m\right| 0_P 0_T > \tag{5}$$

where we are considering the ejection of target nucleons with wave number vectors $\mathbf{k}_j$ into continuum states, and the ground states of the projectile and target are denoted by $|0_P>$ and $|0_T>$, respectively. In equation (5) the eikonal operator $(\widehat{\chi})$ is defined as

$$\widehat{\chi}\left(\mathbf{b}\right) = \frac{1}{(2\pi)^2 k_{\rm NN}}\sum_{\alpha,j}\int_{-\infty}^{\infty} dz\int d^3q\ e^{i\mathbf{q}\cdot\boldsymbol{\eta}}\,e^{-i\mathbf{q}\cdot\mathbf{r}_\alpha}\,e^{i\mathbf{q}\cdot\mathbf{r}_j}\,f_{\rm NN}\left(\mathbf{q}\right) \tag{6}$$

where α and j label the projectile and target constituents, respectively, $\boldsymbol{\eta} = (\mathbf{b}, z)$ is the projectile-target relative separation, $\mathbf{r}$ is the internal nuclear coordinate, $f_{\rm NN}$ is the nucleon-nucleon amplitude, and $k_{\rm NN}$ is the NN relative wave number.

In references 3–5 we showed that if plane-wave states are assumed for $\mathbf{k}_j$, the collision terms are well approximated by

$$W_m\left(\mathbf{R}_\perp,\mathbf{S}_\perp,\omega\right) = \frac{C_m\left(\omega-\epsilon_{B_m}\right)^{m-1}}{(m!)^2}\left[W_1\left(\mathbf{R}_\perp,\mathbf{S}_\perp,\frac{\xi_m}{\sqrt{m}}\right)\right]^m \tag{7}$$

where

$$\mathbf{R}_\perp = \mathbf{b} - \mathbf{b}' \tag{8}$$

and

$$\mathbf{S}_\perp = \frac{1}{2}\left(\mathbf{b} + \mathbf{b}'\right) \tag{9}$$

ϵ_{B_m} is the total binding energy for m knockout nucleons, and the energy-loss parameter is defined as

$$\xi_m = \sqrt{2m_{\rm N}\left(\omega - \epsilon_{B_m}\right)} \tag{10}$$

where $m_{\rm N}$ is the nucleon mass. In equation (7) the approximation is accurate for forward-peaked density matrices, and $C_1 = 1$, $C_2 = \pi/4$, $C_3 = \pi/105$, and $C_4 = \pi^2/240$.

The first collision term is given by

$$W_1\left(\mathbf{b},\mathbf{b}',\omega\right) = \frac{A_P^2 A_T}{(2\pi)^4\, k_{\rm NN}^2} \int_{-\infty}^{\infty} dz \int_{-\infty}^{\infty} dz' \int d^3q\; d^3q'\; e^{i\mathbf{q}\cdot\boldsymbol{\eta}}\, e^{-i\mathbf{q}'\cdot\boldsymbol{\eta}'}$$
$$\times F\left(\mathbf{q}\right)\; F\left(\mathbf{q}'\right)\; f_{\rm NN}\left(\mathbf{q}\right)\; f_{\rm NN}^{\dagger}\left(\mathbf{q}'\right)\; R_1\left(\boldsymbol{\alpha},\boldsymbol{\beta},\omega\right) \tag{11}$$

where F is the one-body form factor of the projectile, and we have defined

$$\boldsymbol{\alpha} = \frac{1}{2}\left(\mathbf{q} + \mathbf{q}'\right) \tag{12}$$

$$\boldsymbol{\beta} = \mathbf{q} - \mathbf{q}' \tag{13}$$

The target one-particle response function for an uncorrelated wave function is written as (refs. 3–5)

$$R_1\left(\boldsymbol{\alpha},\boldsymbol{\beta},\xi_1\right) = \frac{m_N \xi_1}{(2\pi)^2} \int d^3x\; d^3y\; e^{i\boldsymbol{\alpha}\cdot\mathbf{x}} e^{i\boldsymbol{\beta}\cdot\mathbf{y}}\; j_o\left(\xi_1 x\right)\; \rho\left(\mathbf{y} + \frac{\mathbf{x}}{2}, \mathbf{y} - \frac{\mathbf{x}}{2}\right)$$
$$\times \Theta\left(\omega - \epsilon_{B_1}\right) \tag{14}$$

where ρ is the density matrix of the target, j_o is the zeroth-order spherical Bessel function, and Θ is the unit step function.

In order to evaluate the inclusive distribution for charge-exchange reactions, we replace equation (11) by

$$W_1^{ex}\left(\mathbf{R}_\perp,\mathbf{S}_\perp,\omega\right) = \frac{Z_P N_T}{(2\pi)^4\, k_{NN}^2} \int dz\; dz'\; d^3\alpha\; d^3\beta\; e^{i\boldsymbol{\alpha}\cdot\mathbf{R}} e^{i\boldsymbol{\beta}\cdot\mathbf{S}}$$
$$\times F\left(\boldsymbol{\alpha}+\boldsymbol{\beta}/2\right)\, F\left(\boldsymbol{\alpha}-\boldsymbol{\beta}/2\right)\, f_{ex}\left(\boldsymbol{\alpha}+\boldsymbol{\beta}/2\right)\, f_{ex}\left(\boldsymbol{\alpha}-\boldsymbol{\beta}/2\right)$$
$$\times R_1\left(\boldsymbol{\alpha},\boldsymbol{\beta},\omega\right) \tag{15}$$

when the projectile loses one unit of charge, for example, (p,n) or (^{3}He, ^{3}H) reactions. For the inverse reactions (n,p) or (^{3}H, ^{3}He), the factor $Z_P N_T$ is replaced by $N_P Z_T$. In equation (15) we are also making the simple approximation that the target response does not distinguish between (p,p') or (p,n) reactions. Also, the energy loss in equation (15) for the (p,n) reaction is $\omega = E_P - E_n$. If we use equation (1) for the two-body inputs, we have

$$f_{ex}\left(\boldsymbol{\alpha}+\boldsymbol{\beta}/2\right)\, f_{ex}^{\dagger}\left(\boldsymbol{\alpha}-\boldsymbol{\beta}/2\right) = f_{pp}\left(\boldsymbol{\alpha}+\boldsymbol{\beta}/2\right)\, f_{pp}^{\dagger}\left(\boldsymbol{\alpha}-\boldsymbol{\beta}/2\right)$$
$$+ f_{np}\left(\boldsymbol{\alpha}+\boldsymbol{\beta}/2\right)\, f_{np}^{\dagger}\left(\boldsymbol{\alpha}-\boldsymbol{\beta}/2\right)$$
$$- f_{pp}\left(\boldsymbol{\alpha}+\boldsymbol{\beta}/2\right)\, f_{np}^{\dagger}\left(\boldsymbol{\alpha}-\boldsymbol{\beta}/2\right)$$
$$- f_{pp}^{\dagger}\left(\boldsymbol{\alpha}-\boldsymbol{\beta}/2\right)\, f_{np}\left(\boldsymbol{\alpha}+\boldsymbol{\beta}/2\right) \tag{16}$$

The contribution from nucleon ejection before or after charge exchange is approximated by

$$W_2^{ex}\left(\mathbf{R}_\perp, \mathbf{S}_\perp, \omega\right) = \frac{\pi}{16} W_1^{ex}\left(\mathbf{R}_\perp, \mathbf{S}_\perp, \frac{\xi_1}{\sqrt{2}}\right) W_1\left(\mathbf{R}_\perp, \mathbf{S}_\perp, \frac{\xi_1}{\sqrt{2}}\right) \tag{17}$$

which ignores the noncommutativity of the two-body amplitudes. Higher order processes are evaluated similar to equation (17).

Physical Inputs

We next describe the physical inputs for our calculations. If we do not consider spin dependence, the shell model for a harmonic oscillator basis yields the density matrix

$$\begin{aligned}\rho\left(\mathbf{y}+\frac{\mathbf{x}}{2}, \mathbf{y}-\frac{\mathbf{x}}{2}\right) = & \frac{1}{\left(\pi R_T^2\right)^{3/2}} e^{-y^2/R_T^2} e^{-x^2/4R_T^2} \\ & \times \left\{ a_s + 2a_p\left(\frac{y^2}{R_T^2} - \frac{x^2}{4R_T^2}\right)\right. \\ & \left. + a_d\left[\frac{3}{2} - \frac{2}{R_T^2}\left(\mathbf{y}+\frac{\mathbf{x}^2}{4}\right) + \frac{2}{R_T^4}\left(\mathbf{y}^2 - \frac{\mathbf{x}^2}{4}\right)^2\right]\right\}\end{aligned} \tag{18}$$

where R_T is the target matter radii and a_s, a_p, and a_d are normalization constants for s-, p-, and d-shell nucleons, respectively, given (for $A_T \leq 40$) by

$$a_s = \left\{ \begin{array}{ll} \frac{4}{A_T} & (A_T > 4) \\ 1 & (A_T \leq 4) \end{array} \right\} \tag{19}$$

$$3a_p = \left\{ \begin{array}{ll} 0 & (A_T \leq 4) \\ \frac{A_T - 4}{A_T} & (4 > A_T \leq 16) \\ \frac{12}{A_T} & (A_T > 16) \end{array} \right\} \tag{20}$$

$$6a_d = \left\{ \begin{array}{ll} 0 & (A_T \leq 16) \\ \frac{A_T - 16}{A_T} & (A_T > 16) \end{array} \right\} \tag{21}$$

The response function for the $1s$ shell is found as

$$R_s = \frac{m_N a_s R_T}{\alpha\sqrt{\pi}} e^{-R_T^2\beta^2/4} e^{-R_T^2\left(\alpha^2+\xi^2\right)} \sinh\left(2R_T^2\alpha\xi\right) \tag{22}$$

for the $1p$ shell as

$$\begin{aligned} R_p = & \frac{m_N a_p R_T}{\alpha\sqrt{\pi}} \left\{ \left[2 - \frac{1}{2}R_T^2\beta^2 + 2R_T^2\left(\alpha^2+\xi^2\right)\right] \sinh\left(2R_T^2\alpha\xi\right)\right. \\ & \left. - 4R_T^2\alpha\xi \cosh\left(2R_T^2\alpha\xi\right)\right\} e^{-R_T^2\beta^2/4} \\ & \times e^{-R_T^2\left(\alpha^2+\xi^2\right)} \end{aligned} \tag{23}$$

and for the degenerate $1d$ and $2s$ shells, which we have combined as a single shell because spin coordinates are not treated explicitly,

$$
\begin{aligned}
R_d = \frac{m_N a_d R_T}{\alpha\sqrt{\pi}} \Bigg\{ & \left[\frac{7}{2} + 2R_T^2 \left(\alpha^2 + \xi^2\right) + 2R_T^4 \left(\alpha^2 + \xi^2\right)^2 \right. \\
& \left. + \; 8R_T^4 \alpha^2 \xi^2 \right] \sinh\left(2R_T^2 \alpha\xi\right) \\
& - R_T^2 \beta^2 \left[\frac{3}{2} + R_T^2 \left(\alpha^2 + \xi^2\right) \right] \sinh\left(2R_T^2 \alpha\xi\right) \\
& + \frac{1}{8} R_T^4 \beta^4 \sinh\left(2R_T^2 \alpha\xi\right) \\
& - \left[4R_T^2 \alpha\xi + 8R_T^4 \alpha\xi \left(\alpha^2 + \xi^2\right) \right] \cosh\left(2R_T^2 \alpha\xi\right) \\
& + \; 2R_T^4 \beta^2 \alpha\xi \cosh\left(2R_T^2 \alpha\xi\right) \Bigg\} e^{-R_T^2 \beta^2/4} e^{-R_T^2 \left(\alpha^2 + \xi^2\right)}
\end{aligned}
\tag{24}
$$

Values for occupation probabilities calculated from equations (19)–(21) and the radius parameter R_T are listed in table 1. Separation energies for several nuclei are listed in table 2. (See ref. 6.)

Table 1. Shell Model Parameters

Nucleus	a_s	a_p	a_d	R_T, fm
^{4}He	1.0	0	0	1.33
^{6}Li	.57	.143	0	2.11
^{9}Be	.444	.185	0	1.79
^{12}C	.333	.222	0	1.69
^{16}O	.25	.25	0	1.83
^{20}Ne	.20	.20	.033	2.14
^{27}Al	.148	.148	.068	1.91
^{40}Ca	.1	.1	.1	2.10

For the ^{3}He or ^{3}H projectile we use a form factor $F = \exp\left(-\frac{R_P^2}{4} q^2\right)$ with the projectile radii (R_P) of 1.45 fm. The two-body amplitude is parameterized as

$$
f_{\mathrm{NN}}(q) = \frac{\sigma_{\mathrm{NN}} \left(\rho_{\mathrm{NN}} + i\right) k_{\mathrm{NN}}}{4\pi} \exp\left[-\left(\frac{1}{2} B_{\mathrm{NN}} q^2 - \frac{1}{2} C_{\mathrm{NN}} q^4 \right) \right] \tag{25}
$$

where σ_{NN} is the nucleon-nucleon total cross section, ρ_{NN} is the ratio of the real part to the imaginary part of the forward two-body amplitude, and B_{NN} and C_{NN} are slope parameters.

Equation (25) is used to fit experimental data (ref. 2) for the elastic pp and np scattering. By using equation (1), the charge-exchange data are also fitted with the results plotted as the differential cross section versus the Lorentz invariant momentum transfer $-t = q^2$, shown in figure 1 for several energies. The resulting parameters for equation (25) are listed in table 3. The constraint of fitting three sets of data simultaneously does not allow for an accurate fit to the charge-exchange data at all values of momentum transfer, especially at lower energies. This

Table 2. Binding Energies of Shell Model Orbits

Nucleus	Orbit	ϵ_{B_1}, MeV (a)
^{4}He	s	20.5
^{6}Li	s	26.0
	p	5.2
^{9}Be	s	27.2
	p	18.2
^{12}C	s	38.7
	p	17.5
^{16}O	s	39.0
	p	18.0
^{27}Al	s	50.0
	p	22.0
	d	15.0
^{40}Ca	s	51.0
	p	35.0
	d	15.0

[a] Values for ϵ_{B_1} are taken from reference 6.

Table 3. Nucleon-Nucleon Amplitude Parameters

$T_{\rm lab}$, MeV	ρ_{pp}	ρ_{np}	B_{pp}, fm^2	B_{np}, fm^2	C_{pp}, fm^4	C_{np}, fm^4
460	−0.9	0.05	0.008	0.1	0.003	0.005
630	−.54	−.08	.23	.24	.0065	.0075
830	−.06	−.35	.20	.21	.0036	.0036
1000	−.05	−.4	.22	.22	.0036	.0036
2200	−.245	−.496	.29	.282	.0037	.0037

problem, which persists even when more sophisticated parameterizations of the NN amplitudes are used, has been attributed to the need for a description of the charge-exchange reaction using Quantum Chromodynamics (ref. 7). A more conventional explanation to the behavior of the charge-exchange amplitudes than that given in reference 7 is that the amplitude is dominated by one pion exchange with large distortion effects from coupling to the elastic channels (ref. 8). Because we are not considering interference between the amplitudes in the second-order terms, an alternative fit to the charge-exchange data using

$$f_{ex} = \frac{\sigma_{ex} k_{\rm NN}}{4\pi} \exp\left[-\left(\frac{1}{2}B_{ex}q^2 - \frac{1}{2}C_{ex}q^4\right)\right] \tag{26}$$

without regard to equation (1) is also considered; the resulting fits are shown in figure 2 and parameters for several energies are listed in table 4. The charge-exchange distributions shown in figures 1 and 2 are largely independent of shape. This is in contrast to the elastic pp and np data that are nearly isotropic at low energies and show the diffractive forward peak at high energies.

Table 4. Charge-Exchange Amplitude Parameters

T_{lab}, MeV	σ_{ex}, fm^2	B_{ex}, fm^2	C_{ex}, fm^4
260	5.9	0.42	0.02
310	4.27	.42	.022
379	5.02	.42	.02
460	3.89	.36	.0175
545	3.64	.41	.017
630	3.27	.46	.0198
830	2.01	.24	.0065
1000	2.14	.29	.007

Results and Discussion

We next discuss calculations of charge-exchange differential cross sections for proton and ^{3}He projectiles. In the intermediate energy range (100 to 1000 MeV), three mechanisms occur for neutron production in proton-induced reactions. These are (1) neutrons from the intranuclear cascade, (2) neutrons from the charge exchange between the incident proton and a bound neutron, and (3) neutrons created in the formation and decay of isobars. When comparing calculations with experimental results we must keep in mind that only the second mechanism is considered in our calculations. Isobar formation becomes important above an incident projectile energy of about 500 MeV, and neutrons produced at that level will be peaked at energy losses above that corresponding to the pion mass of 139 MeV. Cascade neutrons are those knocked out of the target nucleus and will be produced with an energy spectrum peaked at low energies and extending out to several hundreds of MeV because of multiple collisions. The neutron spectrum from the charge exchange will be peaked at energies close to the incident projectile energy with the isospin transitions to bound excited states (not considered here) occurring in the first few 10's of MeV. The quasi-elastic knockout, which we will consider, occurs at higher excitation energies above the lowest shell separation energies.

In sketch A we compare calculations for 667-MeV protons on ^{27}Al by using the amplitudes of equation (25) (solid line) and equation (26) (dashed line). The improved fit of equation (26) at smaller momentum transfers (see figs. 1 and 2) leads to a larger peak in the cross-section distribution close to the beam energy, whereas at the larger energy losses the results are very similar. This comparison demonstrates the importance of having a correct description of nucleon charge-exchange amplitudes, especially the slope parameters, in describing the production of high-energy neutrons.

In figure 3, calculations are compared with experimental data for neutron production from 450-MeV protons incident on an aluminum target of 6.73 g/cm^2. Figure 3(a) compares the experimental data of reference 9 (the hatched area) with the calculations described above (a solid line for all order terms and a dashed line for the first-order terms) at a neutron production angle of 20°. The histogram shown is the result of the Bertini Monte Carlo model (ref. 9). In figure 3(b) a similar comparison is made for a neutron production angle of 30°. The strengths of the cross-section distributions are predicted quite well by the calculations; however, the peak is shifted to higher energies than the measurements, especially for the comparison at 20°. The Monte Carlo results are also in disagreement with the experimental results. One possibility for the discrepancy may be due to the thickness of the target (6.73 g/cm^2) which presents a nonnegligible possibility for multiple collisions of the incident proton or secondary neutron.

In figure 4 we compare our results with recent experimental data (ref. 10) for $^{12}\mathrm{C}(p,n)X$ reactions at 290 MeV (fig. 4(a)) and 420 MeV (fig. 4(b)) where the cross-section distribution is plotted against energy loss (ω). The solid line denotes the calculation described above through

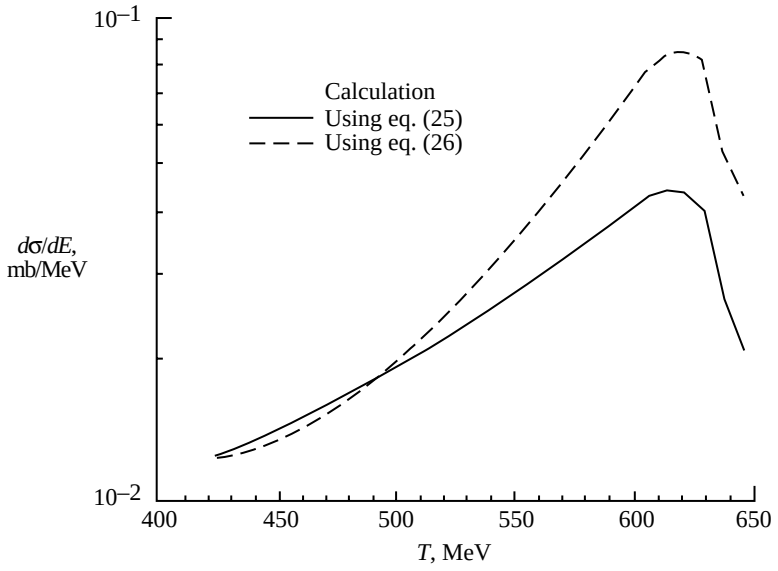

Sketch A

third-order terms and the dashed line denotes a calculation in a relativistic plane-wave model that has been normalized to the data as described in reference 10. Agreement between calculations and experiment is good except where a small energy loss occurs, which may be due to resonance excitation.

In figure 5, predictions for neutron production from the charge exchange for protons incident on ^{16}O and ^{27}Al are made at several energies. We note that the multiple-shell structure of the targets is more apparent at lower incident proton energies because less absorption occurs, and this results in a smaller decrease in the contributions from the lower shells in comparison with the results at higher energies, i.e., at 1 GeV. At all energies the effects of absorption are quite important in reducing the lower shells when compared with the results expected from a plane-wave model (ref. 5).

In figure 6, calculations for the ^{12}C(^{3}He,^{3}H)X reaction for an incident ^{3}He energy of 2 GeV are compared with the data of reference 11 for several triton production angles. Agreement at the forward angles is quite good on the effects of the quasi-elastic background from the pp and np channels, which are seen to be more important than those for incident protons. The agreement at larger angles is poor because of the use of an uncorrelated density matrix that is known to have insufficient strength at large momentum transfers (ref. 12).

Concluding Remarks

A formalism for describing charge-exchange reactions was investigated for light nuclei-induced reactions. Comparisons of the calculations with experimental data for target nuclei most important for space radiation studies were quite favorable for the model considered. Coherent effects were seen to be important for (^{3}He,^{3}H) reactions. Improvements in the calculations will most likely occur when more realistic charge-exchange amplitudes are considered and by the treatment of correlation effects in the nuclear response functions.

NASA Langley Research Center
Hampton, VA 23681-0001
September 17, 1993

References

1. Bianchi, Marilena; Baarli, J.; Sullivan, A. H.; Di Paola, M.; and Quintiliani, M.: RBE Values of 400-MeV and 14-MeV Neutrons Using Various Biological Effects. *Biological Effects of Neutron Irradiation*, International Atomic Energy Agency, 1974, pp. 349–357.

2. Schopper, H., ed.: *Elastic and Charge Exchange Scattering of Elementary Particles. Landolt-Bornstein Numerical Data and Functional Relationships in Science and Technology*, Group I, Volume 7, Springer-Verlag, 1973.

3. Cucinotta, F. A.; Townsend, L. W.; and Wilson, J. W.: *Quasi-Elastic Nuclear Scattering at High Energies.* NASA TM-4362, 1992.

4. Cucinotta, Francis A.; Townsend, Lawrence W.; and Wilson, John W.: Multiple-Scattering Effects in Quasi-Elastic α–^{4}He Scattering. *Phys. Review C*, 3rd ser., vol. 46, no. 4, Oct. 1992, pp. 1451–1456.

5. Cucinotta, F. A.; and Dubey, R. R.: *Final State Interactions and Inclusive Nuclear Collisions.* NASA TP-3353, 1993.

6. Barrett, Roger C.; and Jackson, Daphne F.: *Nuclear Sizes and Structure.* Oxford Univ. Press, 1979.

7. Fernandez, F.; Valcarce, A.; Gonzalez, P.; and Vento, V.: $p(n,p)n$ and $p(p,\Delta^{++})n$ Charge-Exchange Reactions in a Constituent Quark Model. *Phys. Lett.*, vol. B287, no. 1,2,3, 1992, pp. 35–39.

8. Jain, B. K.; and Santra, A. B.: Study of the $p(p,n)\Delta^{++}$ Reaction in Nuclei. *Nucl. Phys.*, vol. A519, 1990, pp. 697–720.

9. Wachter, J. W.; Gibson, W. A.; and Burrus, W. R.: Neutron and Proton Spectra From Targets Bombarded by 450-MeV Protons. *Phys. Review C*, vol. 6, no. 5, Nov. 1972, pp. 1496–1508.

10. Hicks, K. H.; Alford, W. P.; Celler, A.; Henderson, R. S.; Jackson, K. P.; Miller, C. A.; Vetterli, M. C.; Yen, S.; Brieva, F.; Horowitz, C. J.; and Piekarewicz, J.: Comparison of the Quasifree Charge-Exchange Reaction for ^{12}C and ^{54}Fe. *Phys. Review C*, vol. 47, no. 1, Jan. 1993, pp. 260–266.

11. Bergqvist, I.; Brockstedt, A.; Carlen, L.; Ekstrom, L. P.; Jakobsson, B.; Ellegaard, C.; Gaarde, C.; Larsen, J. S.; and Goodman, C.: The (^{3}He,t) Reaction at Intermediate Energies—Spin-Isospin Transitions to States in ^{12}N and ^{13}N. *Nucl. Phys.*, vol. A469, no. 4, Aug. 1987, pp. 648–668.

12. Antonov, A. N.; Hodgson, P. E.; and Petkov, I. Zh.: *Nucleon Momentum and Density Distributions in Nuclei.* Oxford Univ. Press, 1988.

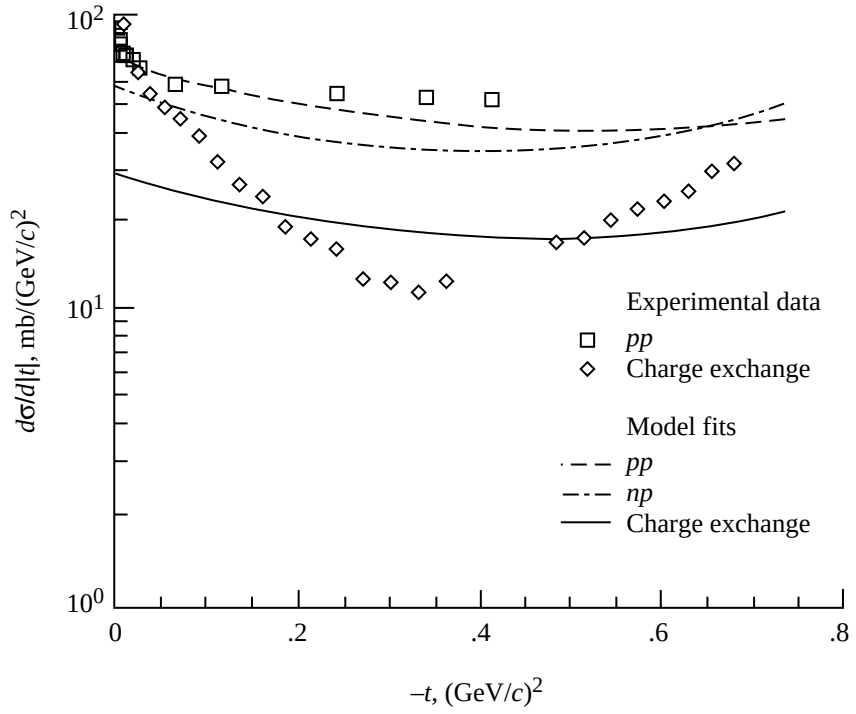

(a) 460 MeV.

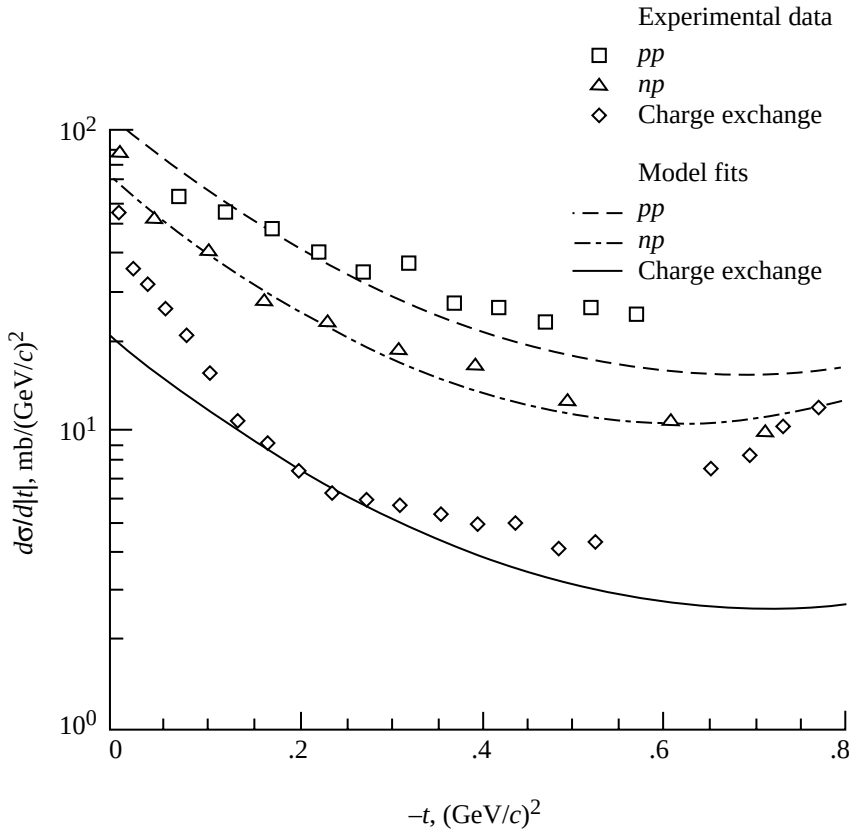

(b) 630 MeV.

Figure 1. Comparison of fits using equation (25) with experimental data (ref. 2) for elastic pp and np scattering and charge-exchange scattering data.

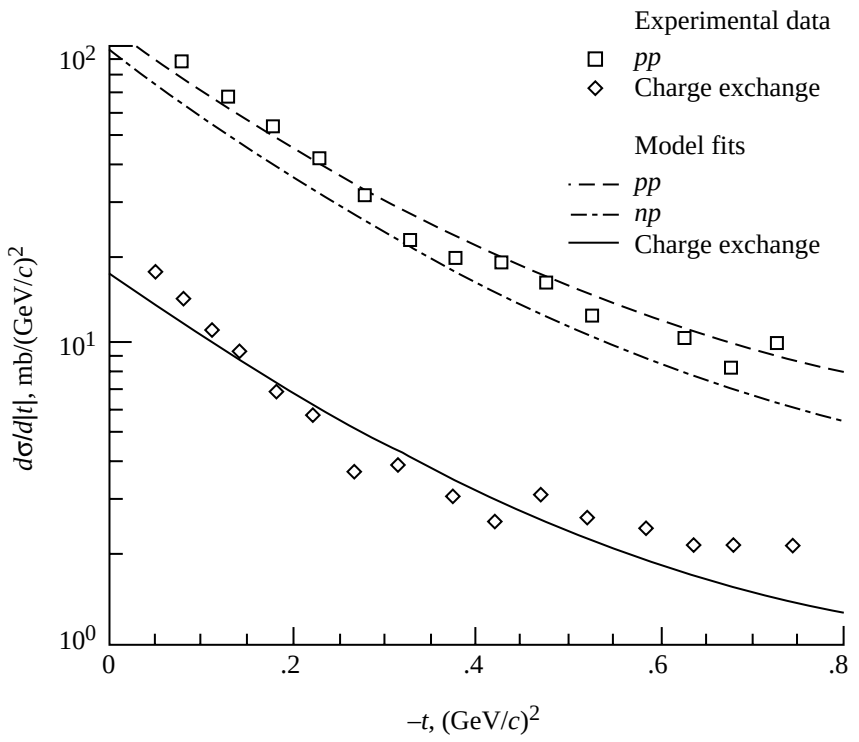

(c) 830 MeV.

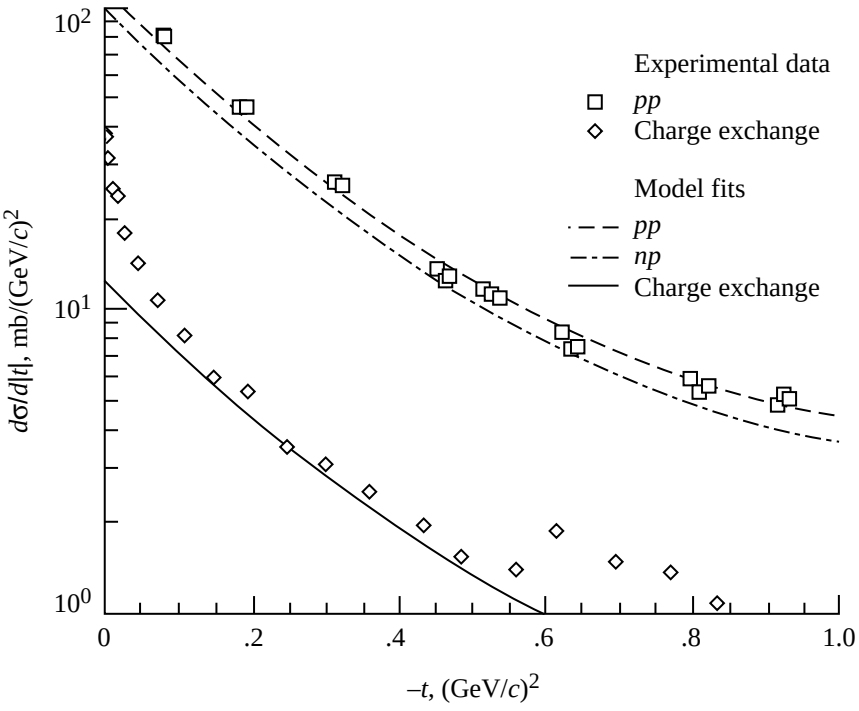

(d) 1000 MeV.

Figure 1. Continued.

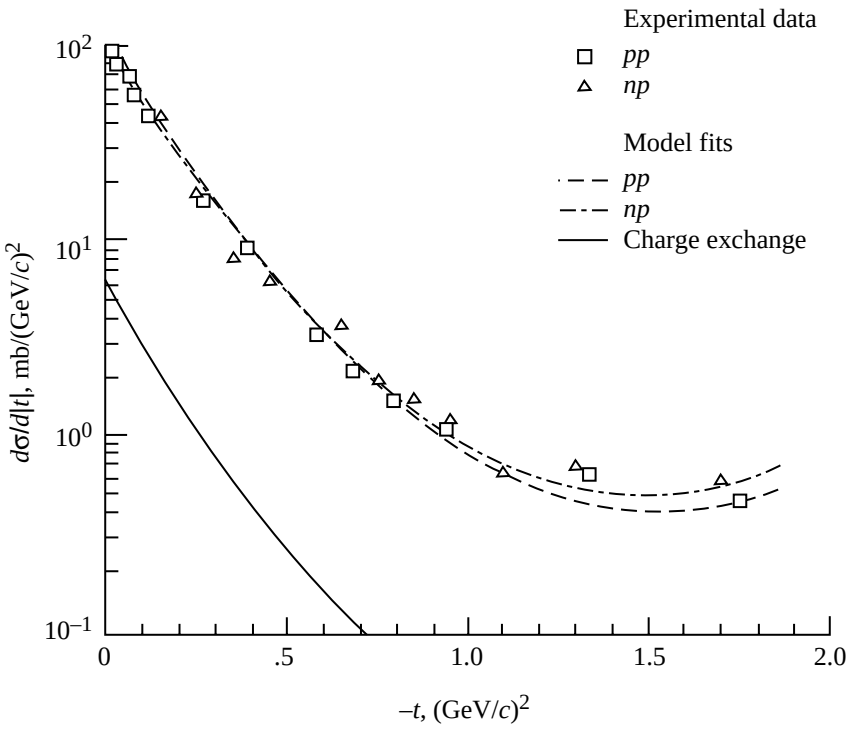

(e) 2000 MeV.

Figure 1. Concluded.

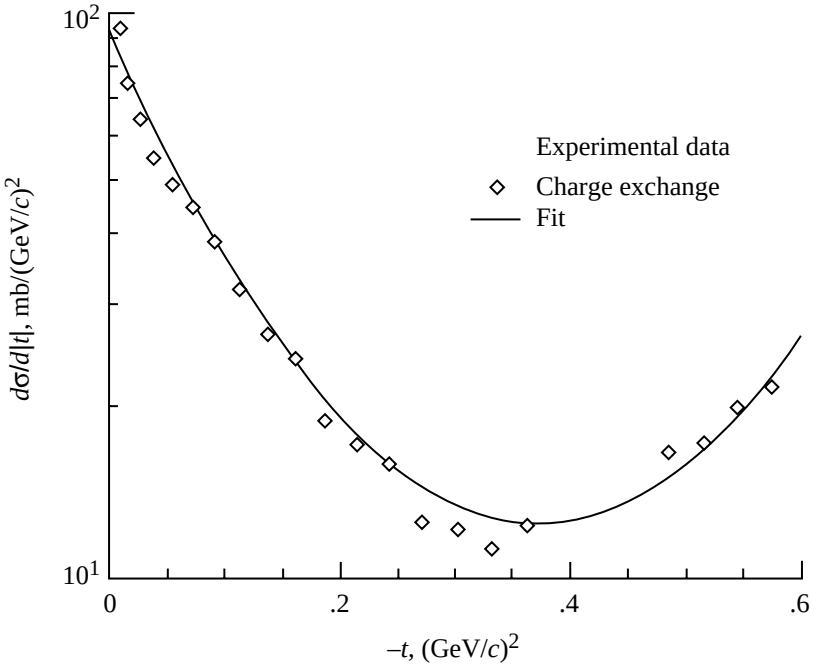

(a) 310 MeV.

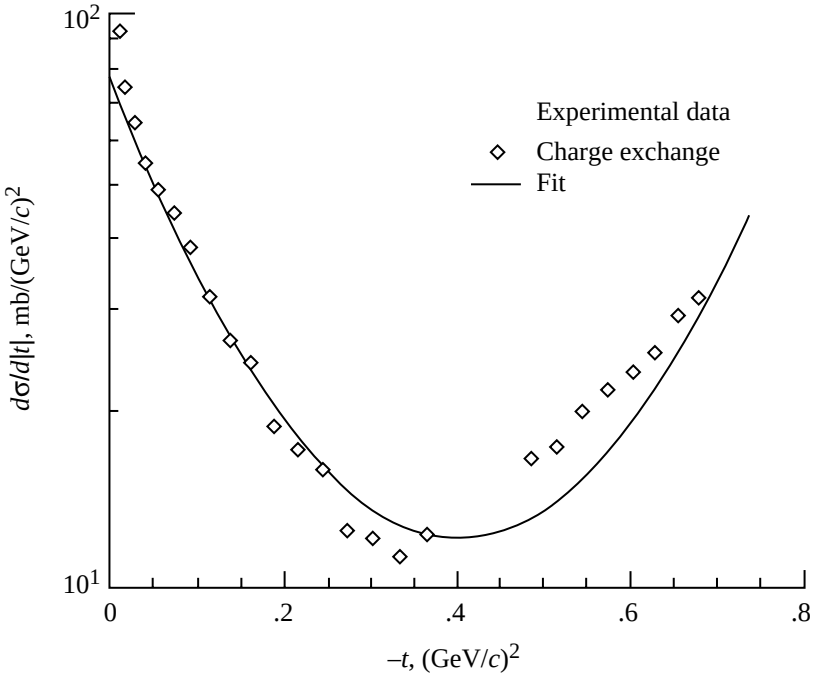

(b) 460 MeV.

Figure 2. Comparison of fits with experimental data (ref. 2) for charge-exchange reactions using equation (26).

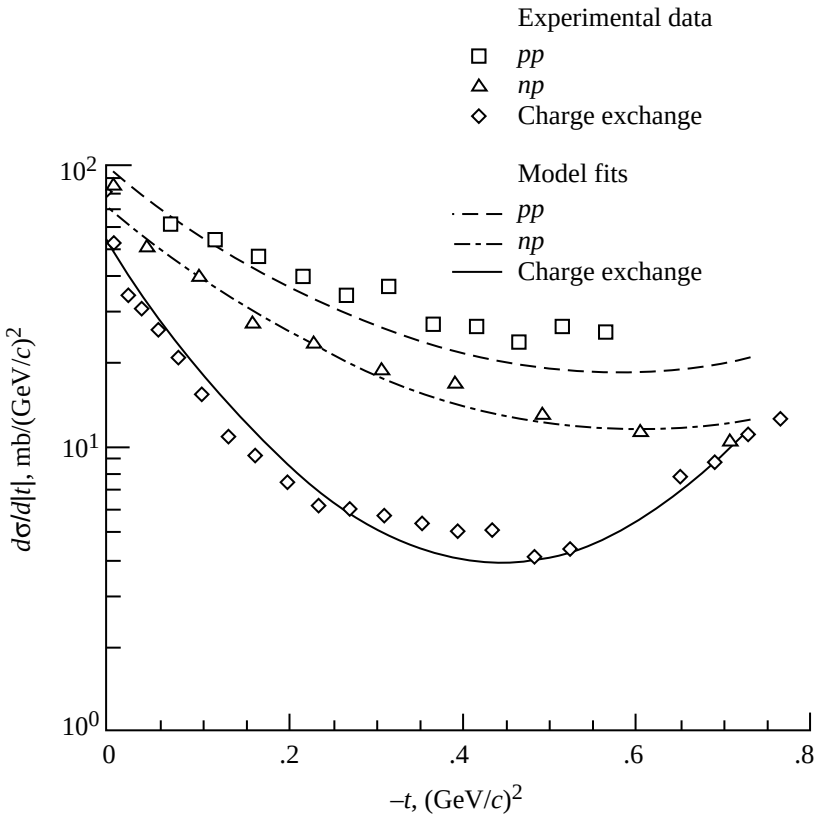

(c) 630 MeV.

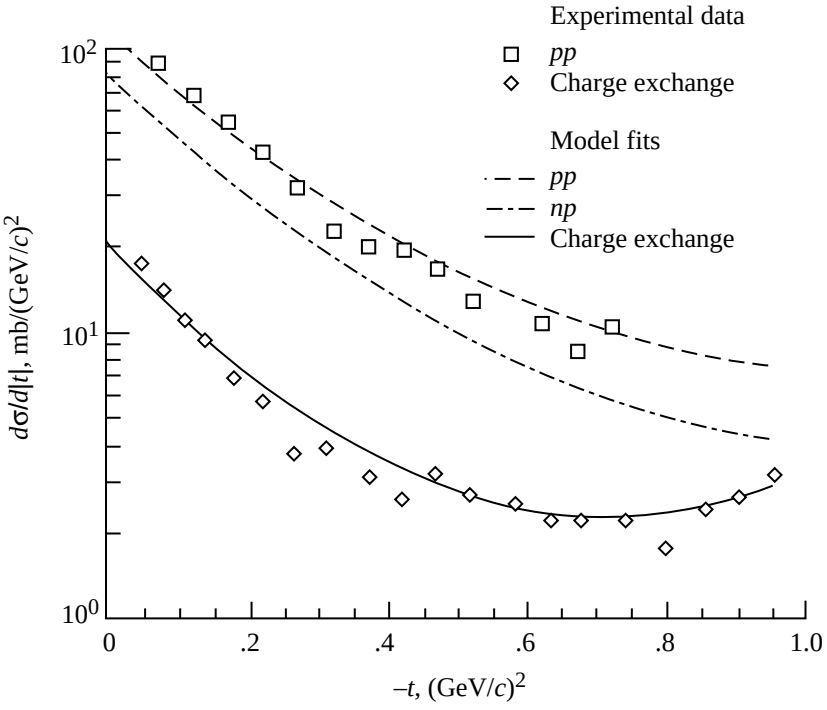

(d) 830 MeV.

Figure 2. Continued.

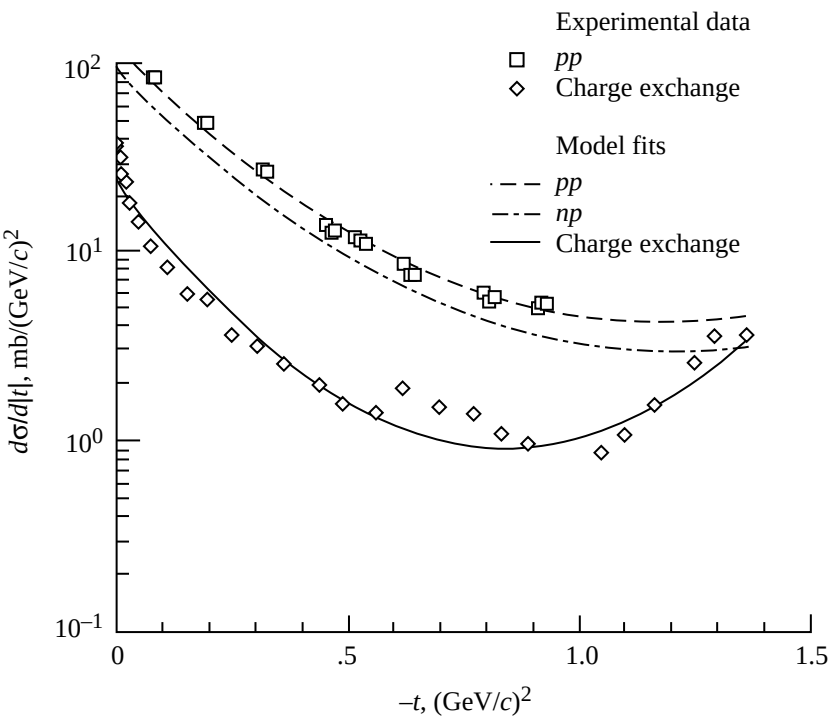

(e) 1000 MeV.

Figure 2. Concluded.

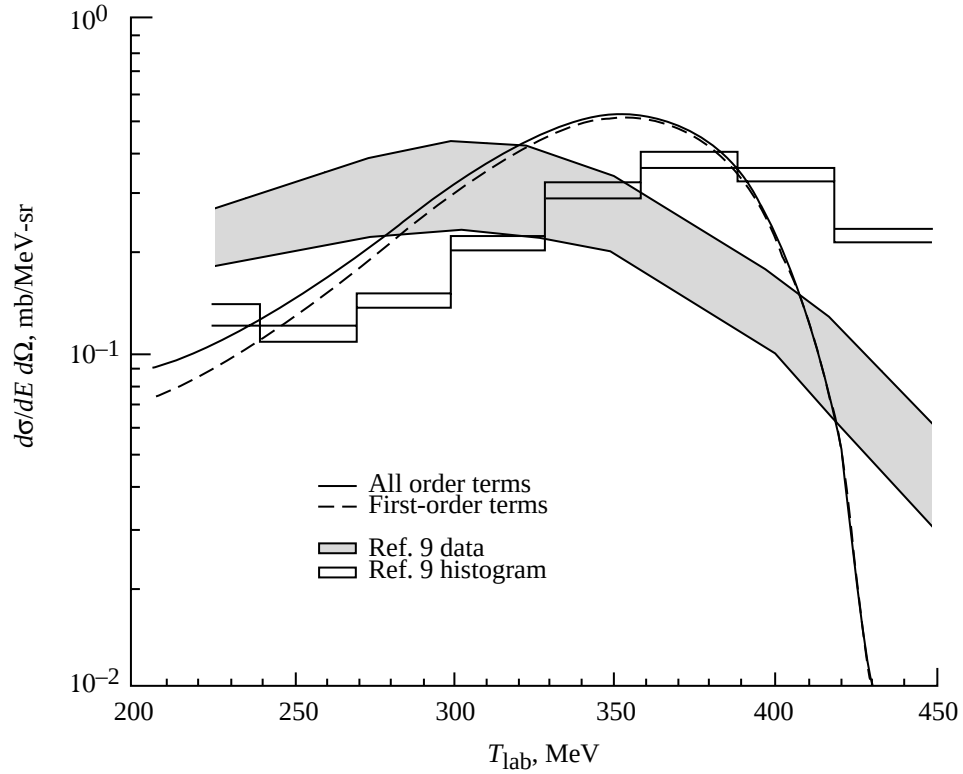

(a) Neutron production angle of 20°.

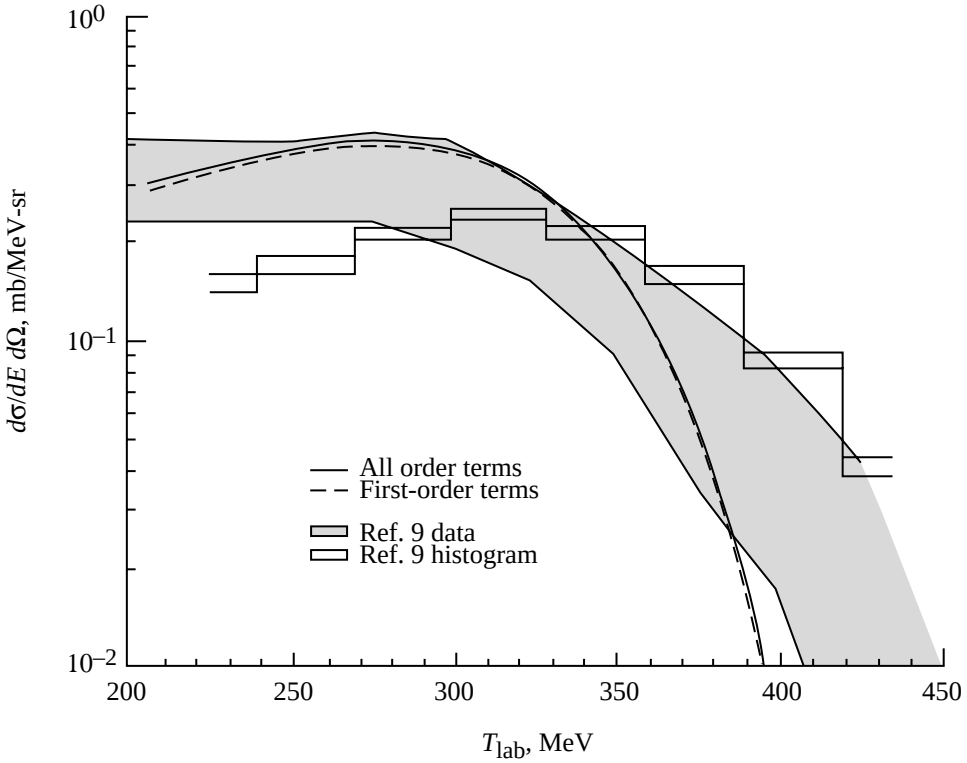

(b) Neutron production angle of 30°.

Figure 3. Comparison of calculations with experimental data of reference 9 for 450-MeV protons on ^{27}Al target of 6.73 g/cm^2.

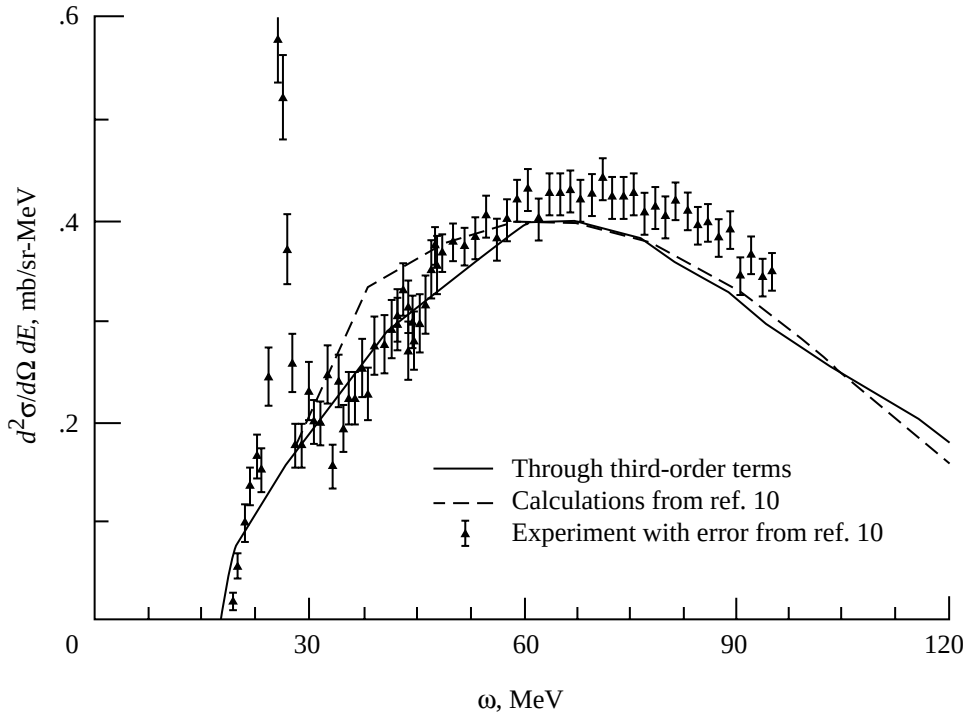

(a) 290 MeV; neutron production angle of 20.4°.

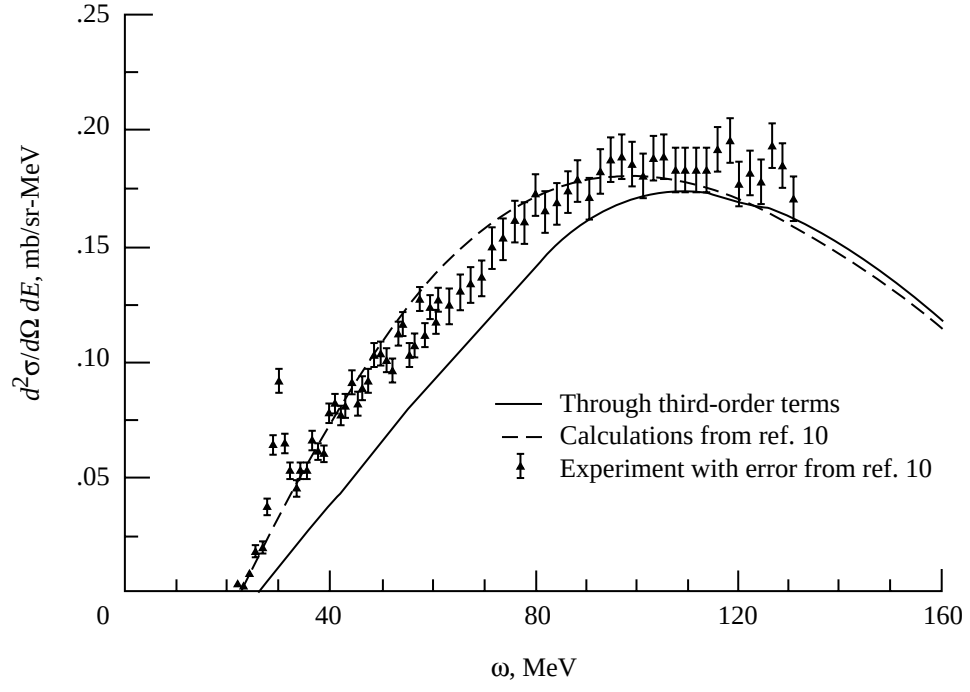

(b) 420 MeV; neutron production angle of 24°.

Figure 4. Comparison of calculations for $^{12}\mathrm{C}(p, n)X$ reaction with experimental data of reference 10.

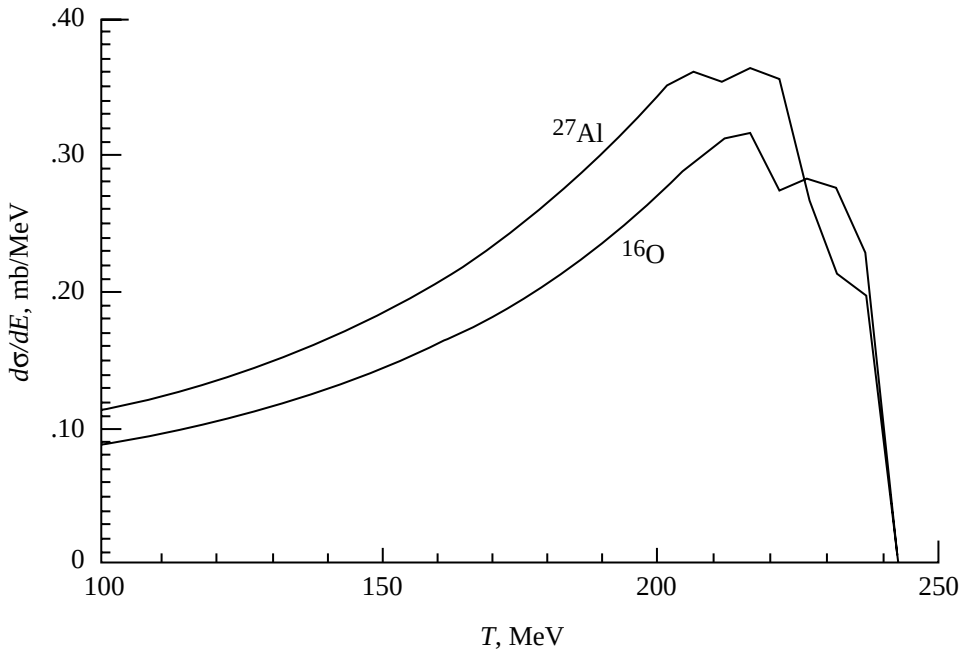

(a) 260 MeV.

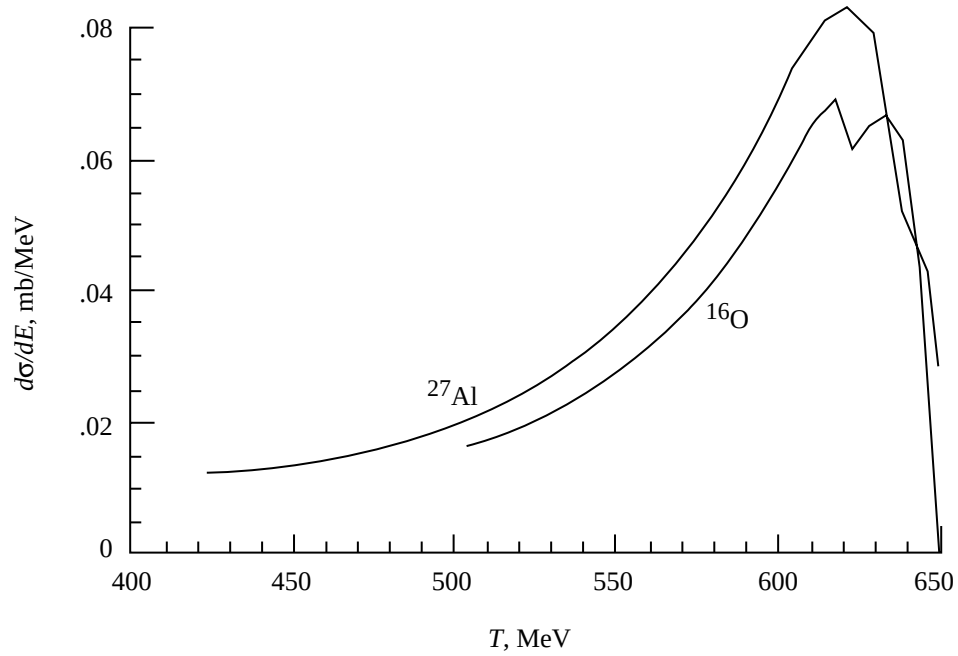

(b) 667 MeV.

Figure 5. Calculations of neutron production in proton collisions on ^{16}O and ^{27}Al.

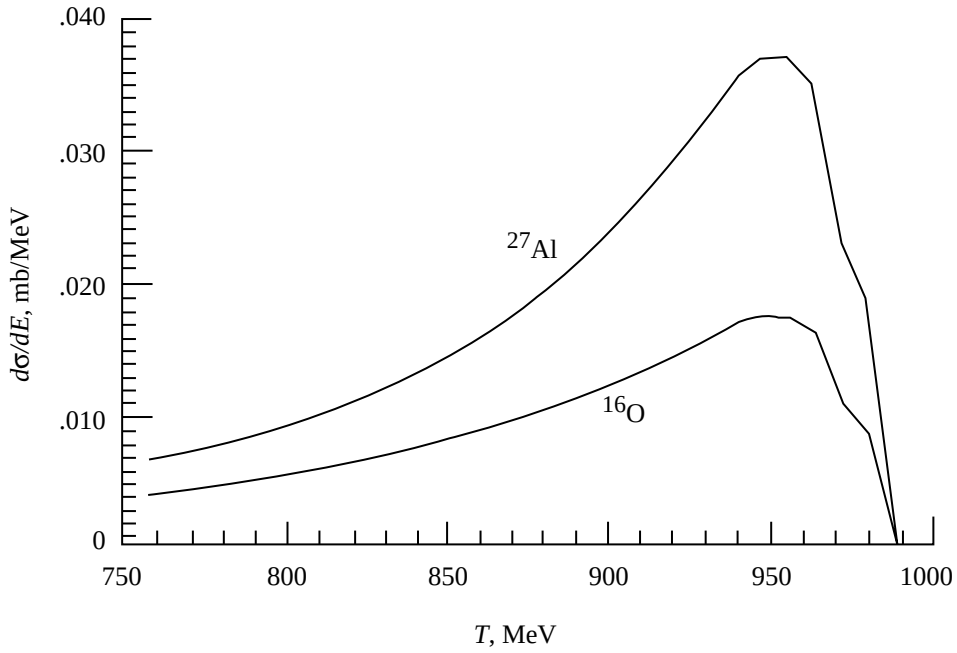

(c) 1000 MeV.

Figure 5. Concluded.

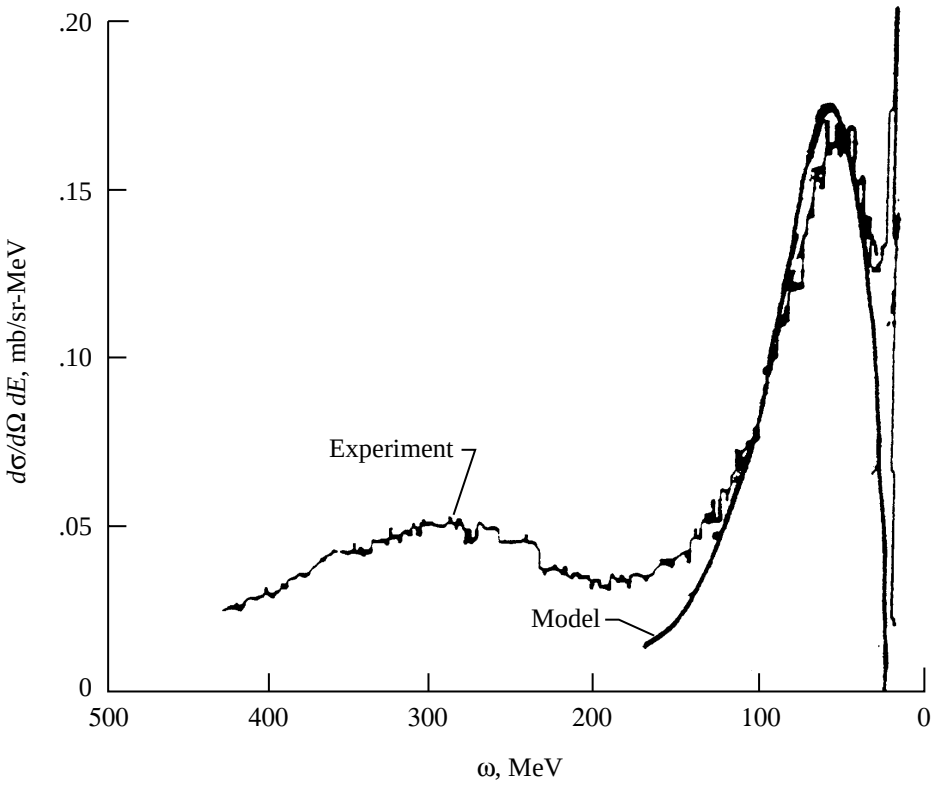

(a) Triton production angle of 4°.

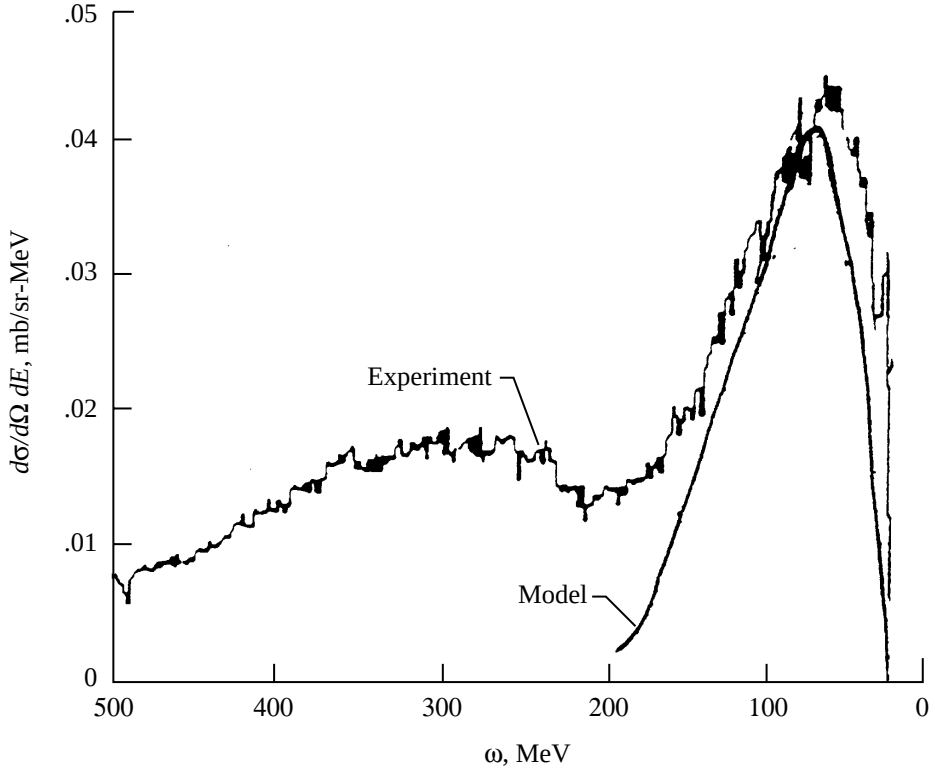

(b) Triton production angle of 5°.

Figure 6. Comparison of calculations for $^{12}\mathrm{C}(^{3}\mathrm{He},^{3}\mathrm{H})X$ reaction at 667 A MeV with experimental data of reference 11.

REPORT DOCUMENTATION PAGE

Form Approved
OMB No. 0704-0188

1. AGENCY USE ONLY *(Leave blank)*	2. REPORT DATE	3. REPORT TYPE AND DATES COVERED
	October 1993	Technical Memorandum

4. TITLE AND SUBTITLE
Energy-Loss Cross Sections for Inclusive Charge-Exchange Reactions at Intermediate Energies

5. FUNDING NUMBERS
WU 199-45-16-11

6. AUTHOR(S)
Francis A. Cucinotta, Lawrence W. Townsend, and Rajendra R. Dubey

7. PERFORMING ORGANIZATION NAME(S) AND ADDRESS(ES)
NASA Langley Research Center
Hampton, VA 23681-0001

8. PERFORMING ORGANIZATION REPORT NUMBER
L-17277

9. SPONSORING/MONITORING AGENCY NAME(S) AND ADDRESS(ES)
National Aeronautics and Space Administration
Washington, DC 20546-0001

10. SPONSORING/MONITORING AGENCY REPORT NUMBER
NASA TM-4522

11. SUPPLEMENTARY NOTES
Cucinotta and Townsend: Langley Research Center, Hampton, VA; Dubey: Old Dominion University, Norfolk, VA.

12a. DISTRIBUTION/AVAILABILITY STATEMENT
Unclassified–Unlimited

Subject Category 73

12b. DISTRIBUTION CODE

13. ABSTRACT *(Maximum 200 words)*
Charge-exchange reactions for scattering to the continuum are considered in a high-energy multiple-scattering model. Calculations for (p, n) and $(^3\mathrm{He}, ^3\mathrm{H})$ reactions are made and compared with experimental results for $^{12}\mathrm{C}$, $^{16}\mathrm{O}$, and $^{27}\mathrm{Al}$ targets. Coherent effects are shown to lead to an important role for inelastic multiple-scattering terms when light projectiles are considered.

14. SUBJECT TERMS
Multiple scattering; High-energy neutrons; Cosmic radiation

15. NUMBER OF PAGES
21

16. PRICE CODE
A03

17. SECURITY CLASSIFICATION OF REPORT	18. SECURITY CLASSIFICATION OF THIS PAGE	19. SECURITY CLASSIFICATION OF ABSTRACT	20. LIMITATION OF ABSTRACT
Unclassified	Unclassified		